MIT
Center for Space Research **Chandra X-Ray Center**

MEMORANDUM
May 3, 2004

To:	Dale Graessle, CALDB lead
From:	Bish K. Ishibashi, SDS
Subject:	Evaluation on the quality of LETG/HRC-S LSFPARM file for unrandomized event datasets
Revision:	1.0
URL:	http://space.mit.edu/CXC/docs/memo_lsf_lh_1.0.ps
File:	/nfs/cxc/h2/bish/CXC SDS/LSFDIR/HO_LSF_HA/memo_lsf_lh_1.0.tex

1 Unrandomized LSFPARM files for LETG/HRC-S Configuration

In Repro *III*, decisions have been made to turn off data randomization on TG R/D. This action necessitates rapid development of line spread function parameter files (LSFPARM) without built-in data randomization. By applying the similar LSF processing scheme[1], new LSFPARM files for LETG+HRC-S configuration have been developed. This document describes the quality of the new LSFPARM products.

2 Building LSFPARM

Procedures for building a LSFPARM file is described at:

> http://space.mit.edu/CXC/LSFX/LSF_valid2.html

For rapid development, several parts of IDL parameterization routines are S-Langified for better and faster convergence to optimum fitting parameters through automated processes.

3 Data products

Two LSFPARM products are developed: LEG $\pm$ 1^{st} orders configuration with LETG+HRC-S without data randomization in TG coordinate. Evaluation of the four products are documented in the following section.

3.1 Header Keyword for Data Randomization

Two new FITS header keywords – RAND_TG and CBD60001 – are included in each LSFPARM product in order to specify whether LSFPARM products is for randomized or not. For unrandomized dataset, these

[1] See an example in https://icxc.harvard.edu/calco/ard_updates/ECR/Approved_ECRs/ECR_2002_016.html

Table 1. New header keywords for LSFPARM

Keyword	Value	Comment
RAND_TG	0.0	No data randomization in TG values
CBD60001	RAND_TG(0.0)	CALDB query expression

header keywords are set to the values as listed in Table 1. These keywords would enable to form proper CALDB query expression and to search for unrandomized LSFPARM products.

3.2 Caveats on Data Randomization in HRC data system

Technically speaking, data randomization adds no effective data blur when applied onto any dataset taken with HRC detectors[2]. Hence the existing LSFPARM for LETG+HRC-S may be valid to both randomized and unrandomized LETG+HRC-S datasets.
However, the old products contain LSFPARM with only one extraction width, hence limiting the way any LETG+HRC-S dataset is calibrated for analysis. The new products contains, however, contains ten different extraction widths, hence making it more versatile for custom extraction by users.

4 Testing LSFPARM products

4.1 Procedures

Testing of the LSFPARM products are performed with MARX simulated and real Capella (ObsID 1248) datasets. Two key points of our interests are (1) line profile and (2) encircled energy fractions (hereafter EEFRAC).

4.2 Evaluation I. MARX-Simulated Dataset

Mono-energetic beam simulations are performed with MARX at various energy values and concatenated together to make a L1 event file. The L1 file has gone through nominal CIAO processing, except that pixel randomization in TG space being turned off at *tg_resolve_events*. Corresponding grating RMF files are generated via *mkgrmf* command with the new LSFPARM files and used as a fitting kernel in *ISIS* for evaluation. Cash statistics is applied throughout this work.

4.2.1 Line Profile Analysis

If the LSFPARM products are valid, simulated line profiles can be described with a Kronecker delta function folded over grating RMFs. Figures 1 and 2 show several line profiles fitted with a delta function. For brevity, selected six of 14 line samples are shown in each figure for inspection: lines at E = 80, 120, 275, 450, 800, and 1500 eV. These are representative of the results of other line profile fittings, resulting in the value of goodness of fit generally less than 1.5 for LEG (these are not meant to be necessarily the best fitting results).

Despite unusually high S/N ratio in these line profile simulations, the model fitting has resulted in the low χ^2 values and hence the results validate that the LSF parameterization works here just as well as with the HETG configuration system.

4.2.2 Encircled Energy Fraction

The second key component of LSFPARM products is the value of encircled energy fraction as a function of energy. The value EEFRAC is derived from cross-dispersion line profile of a mono-energetic beam, integrated over arbitrary extraction width centered around the line peak (or in Chandra's term, at TG_D = 0 degree). If derived correctly, EEFRAC will allow users to correct measured count rates (or fluxes) for the aperture of the extraction.

[2] http://hea-www.harvard.edu/~jdrake/memo/random/

The following tests are performed such that the simulated line spectra (samples shown in Figures 1 and 2) are extracted at three different aperture widths; then the delta-function model is fitted to 14 mono-energetic lines in order to derive model line fluxes F_m in counts s^{-1}. ISIS is also enabled to provide cumulative counts in each line, which is used to derive a "observed" line flux F_d. In an ideal condition, both the model and observed line fluxes should be identical, i.e.,

$$\frac{F_d}{F_m} \approx 1.$$

Two LEG configurations (LEG $\pm$ 1st) are tested and verified that the new LSFPARM products meet this criterion within a few percentage (see Tables 2 and 3), presumably better than our knowledge in effective area of Chandra's HRMA system.

4.3 Evaluation II. Chandra Dataset

The same four LSFPARM products are tested against real Chandra observation (Capella, ObsID = 1248) in the similar manner as performed on the simulated datasets.

4.3.1 Line Profile Analysis

Instead of using a delta function, thermal X-ray APED model and simple Gaussian function are fitted on the emission spectrum of Capella. Eight to ten bright emission lines – Mg XII (λ 8.421), Fe XVII ($\lambda\lambda$ 15.014 and 103.937), O VIII (λ 18.9), N VII (λ 24.78), Fe XIX ($\lambda\lambda$ 45.0328 and 108.37), Fe XVI (λ 54.728), Fe XVIII (λ 93.923), and Fe IX (λ 171.073) – are selected for testing. Upon fitting the parameter for line width dv (converted to velocity scale in km s^{-1}) is allowed to vary. Ideally the parameter dv should be ≈ 0 km s^{-1} for thermal APED modeling; however, for Gaussian fitting, the value dv is expected to be ≥ 0 km s^{-1} as most of these lines are either H-like doublet lines or blended with other weak atomic lines. The results of fitting with the APED model is tabulated in Tables 4 and 5; likewise, the results with the Gaussian model in Tables 6 and 7. Corresponding figures for line profile fit are shown in Figures 3 and 4 for the APED model and in Figures 5 and 6 for the Gaussian model . These are, once again, not meant to be the best fitting parameters.

Upon inspection of Tables 4 and 5, it is noted that the measured line width is consistent with 0 km s^{-1} for the most of lines. Several measured lines in the outer plate show non-zero widths, although the width is below the resolution limit ($\sim$ 0.05Å). One exception is a a N VII λ 24.78 that show a broader width ($\sim$ 300km s^{-1}, including the range of error into consideration) in all of the line measurements. It is possible that this particular line originates from the extended region of stellar coronae.

The same practice with the Gaussian model is repeated and their results show all positive measured line widths, which is expected from blended lines. However the measured widths are not considerably broad (i.e., not greater than 100 km s^{-1}), except for the N VII line in LEG -1st order.

Figures 3 – 6 show the results of line profile fitting. While the strongest line, Fe XVII λ 15.014, shows some significant residuals in all the line models, other line profile models have resulted in a reasonably good fit. It is not clear that my model for the Fe XVII is quite adequate; furthermore, the model fit to the simulated line near 15Ådoes not show any significant residual. Hence this particular line model needs to be re-evaluated first via a collaboration with LETG+HRC. If the model is determined to be correct, then the MARX model may need to be improved to account for the discrepancy.

In any other cases, the LSFPARM products can provide decent description of the observed line profiles.

4.3.2 Encircled Energy Fraction

Lastly the model EEFRAC values need to be compared with the observed ones. Here we first compute the theoretical EEFRAC values at three different aperture widths based on the new LSFPARM products. Then at the same aperture widths extract spectra from observed event datasets. The same Capella dataset (ObsID

1248) is chosen for this exercise. Since absolute spectral energy distributions of the target is not known, the ratio of two entities are compared instead. Here in this exercise, the ratio of the observed spectra "Extraction B" (at a width equivalent to EEFRAC = 80% at E = 1.497keV) to "Extraction A" (similarly at EEFRAC = 90.5%, or nearly at CIAO default extraction width) is compared with the theoretical counterpart. The same exercise is repeated for "Extraction C" (at EEFRAC = 60%) as well.

Due to high detector background noise, the background events are measured and subtracted out prior to the analysis. Furthermore, the total cumulative counts in this dataset is fairly low and therefore the ratio value may blow up at several bins as the numerator being divided by zero. For that reason, the comparisons are made in a base-10 logarithmic space.

If the EEFRAC values in the LSFPARM products are derived properly, the ratio (as a function of wavelength) should be consistent to each other. Figure 7 shows the ratio plots for every LETG configuration derived with the Capella dataset. As shown in the figure, the model trend agrees fairly well with the observed trend for all cases.

5 Summary

All the testings show that the quality of these new LSFPARM products for unrandomized datasets are equally as good as the other LSFPARM products produced through the same LSF generation scheme. While some anomalous differences are found in both line profile and EEFRAC analyses, the difference may originate due to some unidentified calibration issues not included in the current MARX distribution.

Table 2. LEG +1st: the Data-to-Model flux ratio

Energy (eV)	Widths (radian)		
	2.79e-4	1.60e-3	1.84e-2
80	1.01	1.00	1.00
90	1.01	1.05	1.00
100	1.02	1.00	1.01
120	1.01	1.00	1.00
200	1.01	1.00	1.00
275	1.01	1.00	1.00
350	1.01	1.00	1.00
450	1.00	1.00	1.00
600	1.01	1.01	1.01
800	1.00	1.00	1.00
1000	1.00	1.05	1.00
1200	1.00	1.00	1.00
1500	1.00	1.00	1.00
2000	1.00	1.00	1.00

Table 3. LEG -1st: the Data-to-Model flux ratio

Energy (eV)	Widths (radian)		
	2.79e-4	1.60e-3	1.84e-2
80	1.01	1.01	1.01
90	1.01	1.01	1.01
100	1.01	1.00	1.00
120	1.01	1.01	1.01
200	1.01	1.00	1.00
275	1.00	1.00	1.00
350	1.00	1.00	1.00
450	1.00	1.00	1.00
600	1.00	1.00	1.00
800	1.00	1.00	1.00
1000	1.04	1.02	1.02
1200	1.00	1.00	1.00
1500	1.00	1.00	1.00
2000	1.00	1.00	1.00

Table 4. Capella LEG +1st: thermal APED model.

Element	λ_{lab} (Å)	dv (km/s)	dv 3σ range	χ^2	Comment
Mg XII	8.4192	0	0 – 200	1.34	H-like doublet lines
Fe XVII	15.014	0	0 – 47.6	9.21	Seems blended with an unidentified line
O VIII	18.90	0	0 – 103	3.34	H-like doublet lines
N VII	24.78	0	0 – 281	2.06	Extended line emission?
Fe XIX	45.0328	0	0 – 135	0.994	blended with Fe XXIV?
Fe XVI	54.7280	0	0 – 113	1.49	
Fe XVIII	93.923	18.8	0 – 55.4	1.54	
Fe XVII	103.937	73.4	34.4 – 106	1.31	
Fe XIX	108.37	88.0	29.8 – 101	1.02	
Fe IX	171.073	76.6	29.5 – 140	1.13	

Table 5. Capella LEG -1st: thermal APED model.

Element	λ_{lab} (Å)	dv (km/s)	dv 3σ range	χ^2	Comment
Mg XII	8.4192	54.0	0 – 651	0.99	H-like doublet lines
Fe XVII	15.014	8.75	0 – 166	5.47	Seems blended with an unidentified line
O VIII	18.90	0	0 – 106	3.46	H-like doublet lines
N VII	24.78	294	150 – 455	1.07	Extended line emission?
Fe XIX	45.0328	0	0 – 141	1.11	blended with Fe XXIV?
Fe XVI	54.7280	–	–	–	chip gap
Fe XVIII	93.923	25.0	0 – 71.5	1.33	
Fe XVII	103.937	66.0	0 – 93.4	1.35	
Fe XIX	108.37	45.4	0 – 77.0	1.26	
Fe IX	171.073	–	–	–	out of chip

Table 6. Capella LEG +1st: Simple Gaussian model.

Element	λ_{lab} (Å)	dv (km/s)	dv 3σ range	χ^2	Comment
Mg XII	8.4192	61.2	0 – 441	1.29	H-like doublet lines
Fe XVII	15.014	42.1	0.78 – 86.4	11.0	Seems blended with an unidentified line
O VIII	18.90	9.48	0 – 98.1	2.86	H-like doublet lines
N VII	24.78	10.5	9 – 126	1.09	Extended line emission?
Fe XIX	45.0328	14.0	0.20 – 122	0.906	blended with Fe XXIV?
Fe XVI	54.7280	0.414	0 – 98.8	1.42	
Fe XVIII	93.923	32.8	17.3 – 51.0	1.86	
Fe XVII	103.937	55.1	28.5 – 78.7	1.35	
Fe XIX	108.37	64.3	49.2 – 79.7	0.975	
Fe IX	171.073	66.4	33.9 – 95.4	1.12	

Table 7. Capella LEG -1st: Simple Gaussian model.

Element	λ_{lab} (Å)	dv (km/s)	dv 3σ range	χ^2	Comment
Mg XII	8.4192	103	0 – 496	1.28	H-like doublet lines
Fe XVII	15.014	3.73	0 – 144	3.21	Seems blended with an unidentified line
O VIII	18.90	112	0 – 171	1.72	H-like doublet lines
N VII	24.78	237	109 – 361	1.18	Extended line emission?
Fe XIX	45.0328	76.2	0.21 – 143	0.758	blended with Fe XXIV?
Fe XVI	54.7280	–	–	–	chip gap
Fe XVIII	93.923	44.7	28.8 – 58.6	1.55	
Fe XVII	103.937	47.6	21.7 – 73.8	1.44	
Fe XIX	108.37	48.9	32.9 – 65.2	1.25	
Fe IX	171.073	–	–	–	out of chip

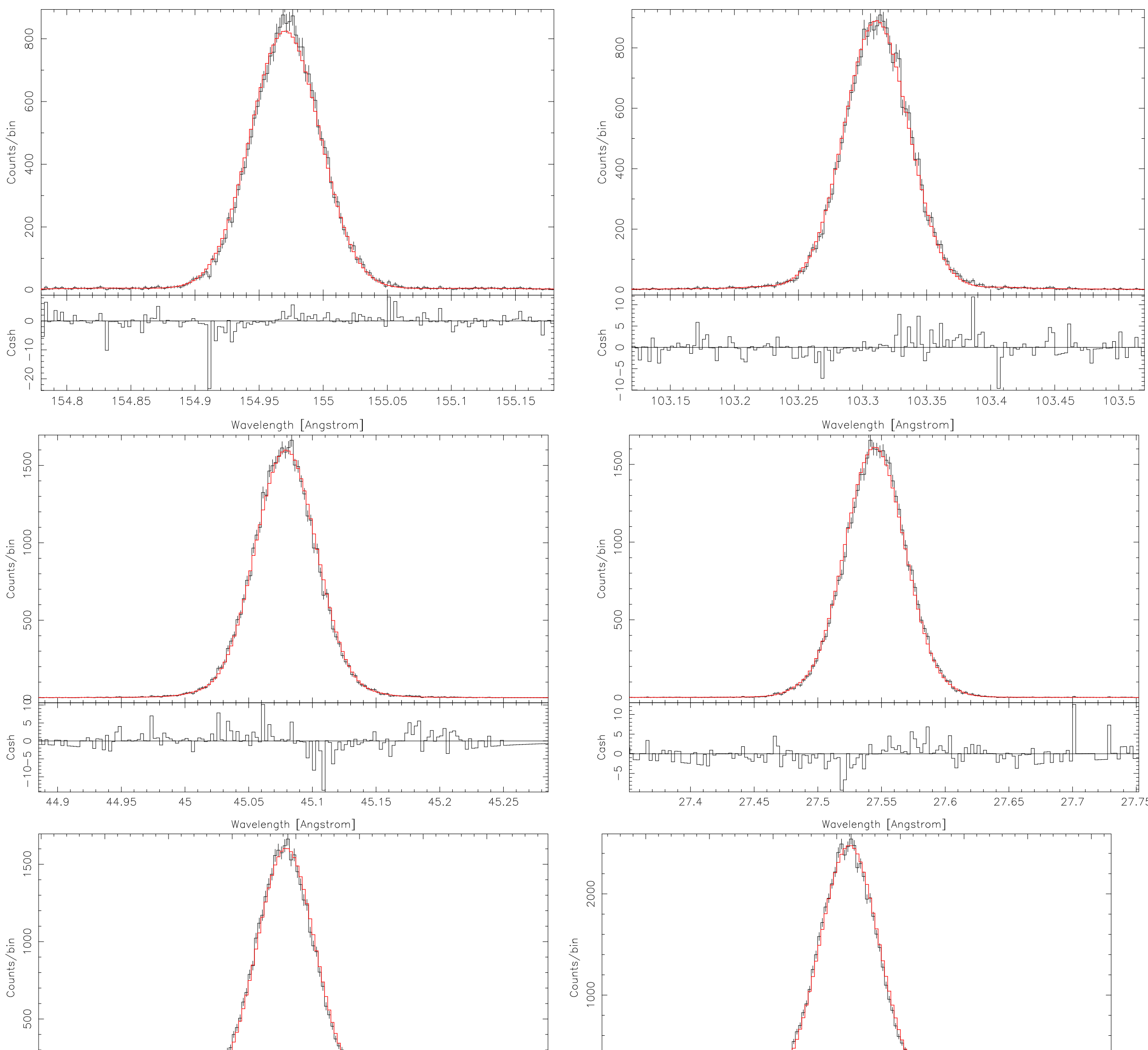

Figure 1: LEG +1st-order line profiles, fitted with a Kronecker delta function (red) folded over LEG +1st through +11st multi-order grating RMFs: (top right) line profile at E = 80 eV, with a goodness of fit χ^2 = 1.38; (top left) E = 120 eV, χ^2 = 1.40; (middle left) E = 275 eV, χ^2 = 1.47; (middle right) E = 450 eV, χ^2 = 1.40; (bottom right) E = 800 eV,χ^2 =2.00; and (bottom left) E = 1500 eV, χ^2 = 0.966. The delta function model describes simulated line profiles fairly well.

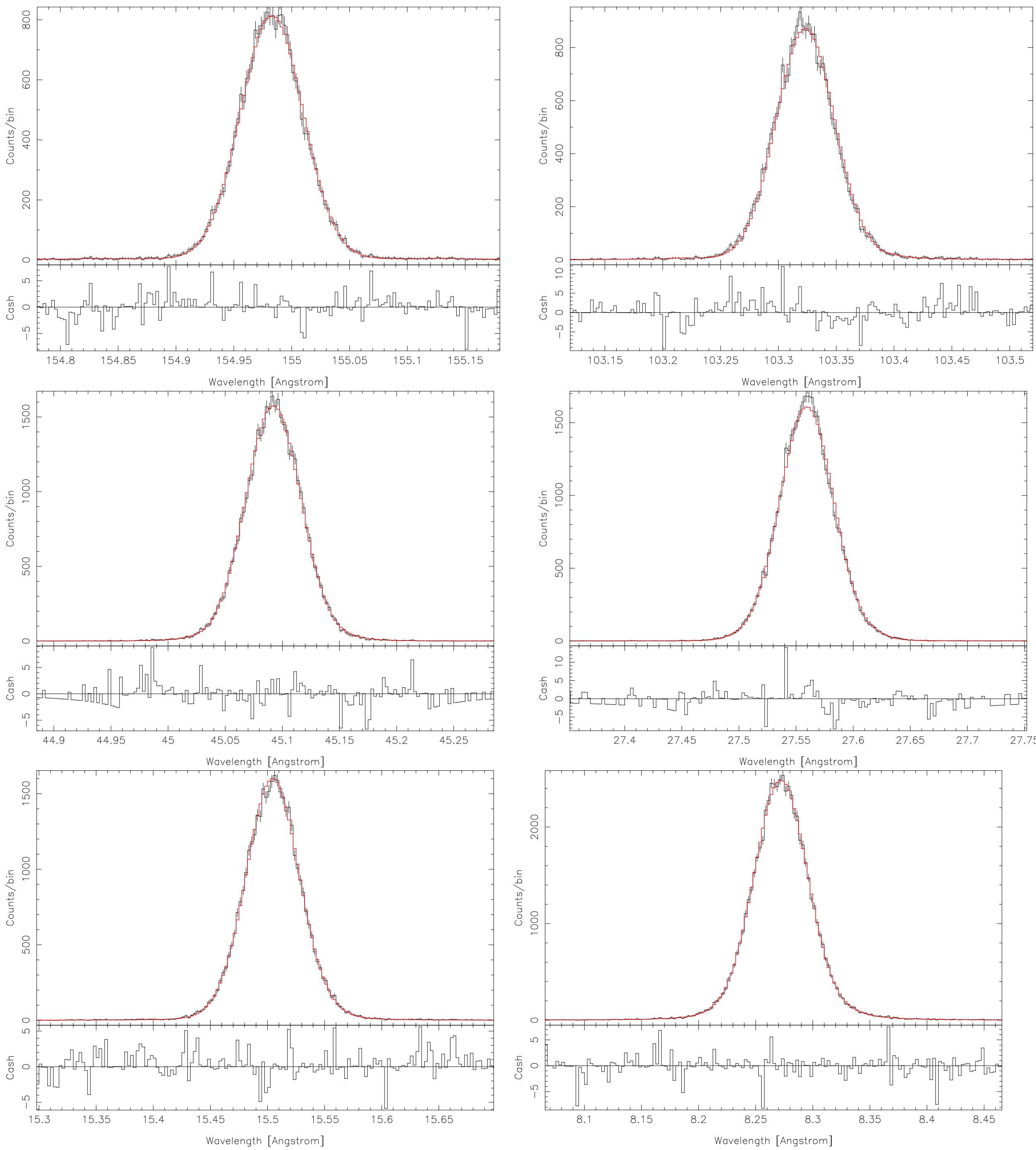

Figure 2: LEG +1st-order line profiles: (top right) line profile at E = 80 eV, with a goodness of fit χ^2 = 1.21; (top left) E = 120 eV, χ^2 = 1.68; (middle left) E = 275 eV, χ^2 = 1.27; (middle right) E = 450 eV, χ^2 = 1.29; (bottom right) E = 800 eV,χ^2 =1.12; and (bottom left) E = 1500 eV, χ^2 = 1.53.

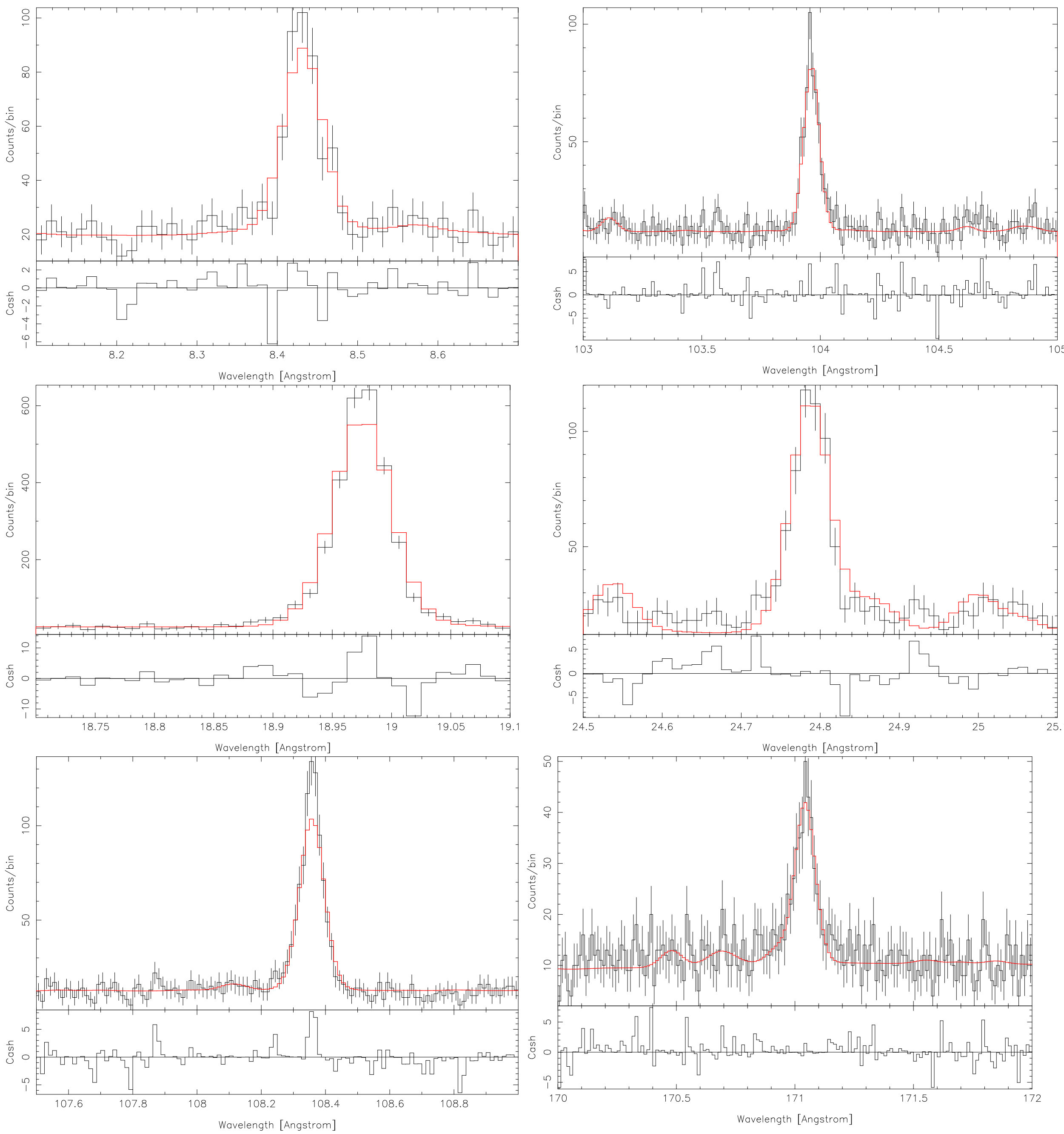

Figure 3: Selected LEG +1st-order Capella line profiles; (top left) Mg XII line, fitted with an APED thermal model (red) and its goodness of fit $\chi^2 = 1.34$; (top right) Fe XVII with $\chi^2 = 9.21$; (middle left) O VIII with $\chi^2 = 3.34$; (middle right) N VII with $\chi^2 = 2.06$; (bottom left) Fe XIX with $\chi^2 = 1.02$; and (bottom right) Fe IX with $\chi^2 = 1.13$. This simplified APED model (not necessarily the best fit) adequately describes the Capella line spectra, though the atomic model may be lacking in its accuracy, which lead to higher χ^2 values.

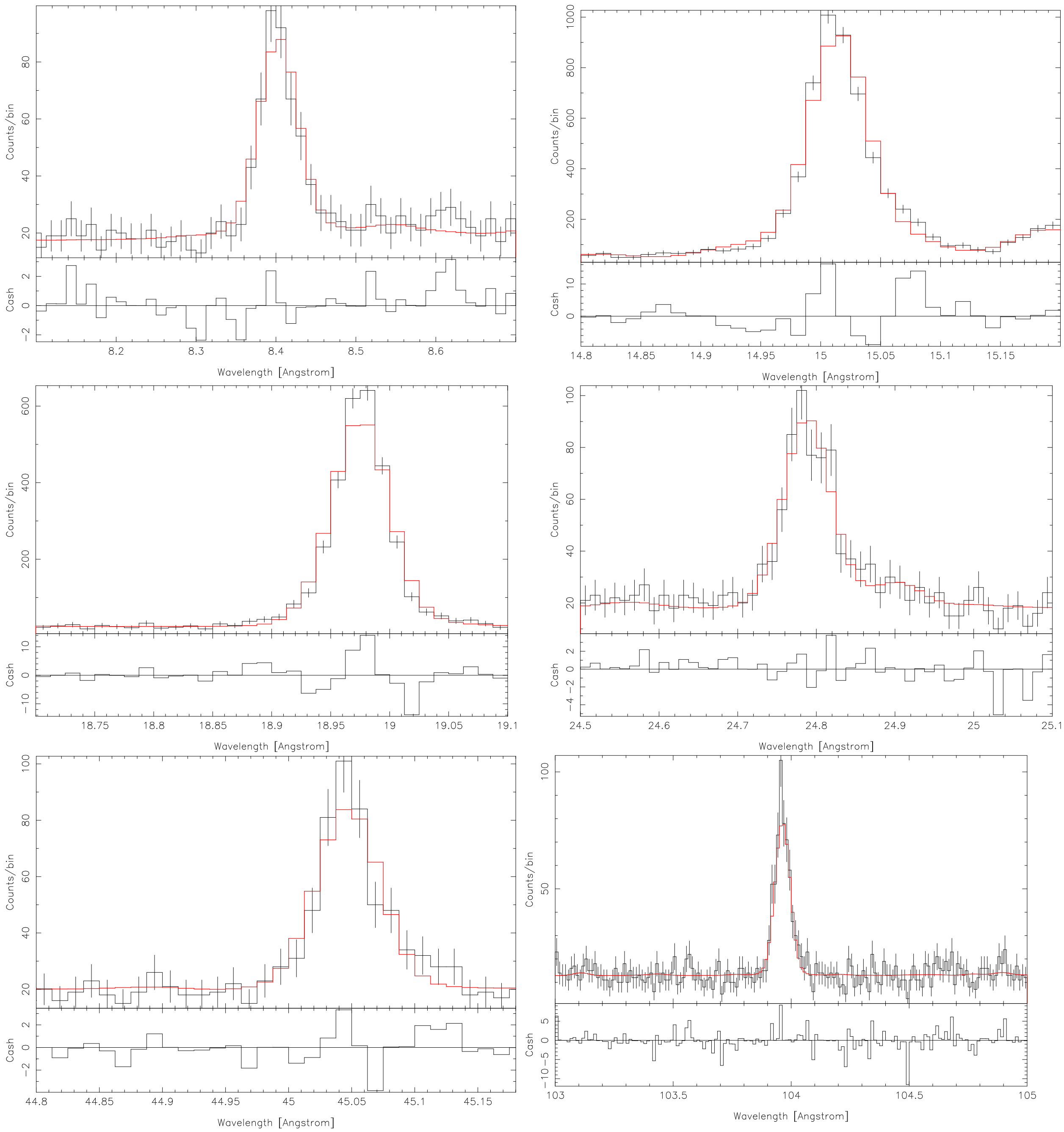

Figure 4: Selected LEG -1st-order Capella line profiles; (top left) Mg XII line, fitted with an APED thermal model (red) and its goodness of fit $\chi^2 = 0.99$; (top right) Fe XVII with $\chi^2 = 5.47$; (middle left) O VIII with $\chi^2 = 3.46$; (middle right) N VII with $\chi^2 = 1.07$; (bottom left) Fe XIX with $\chi^2 = 0.758$; and (bottom right) Fe XVII with $\chi^2 = 1.35$.

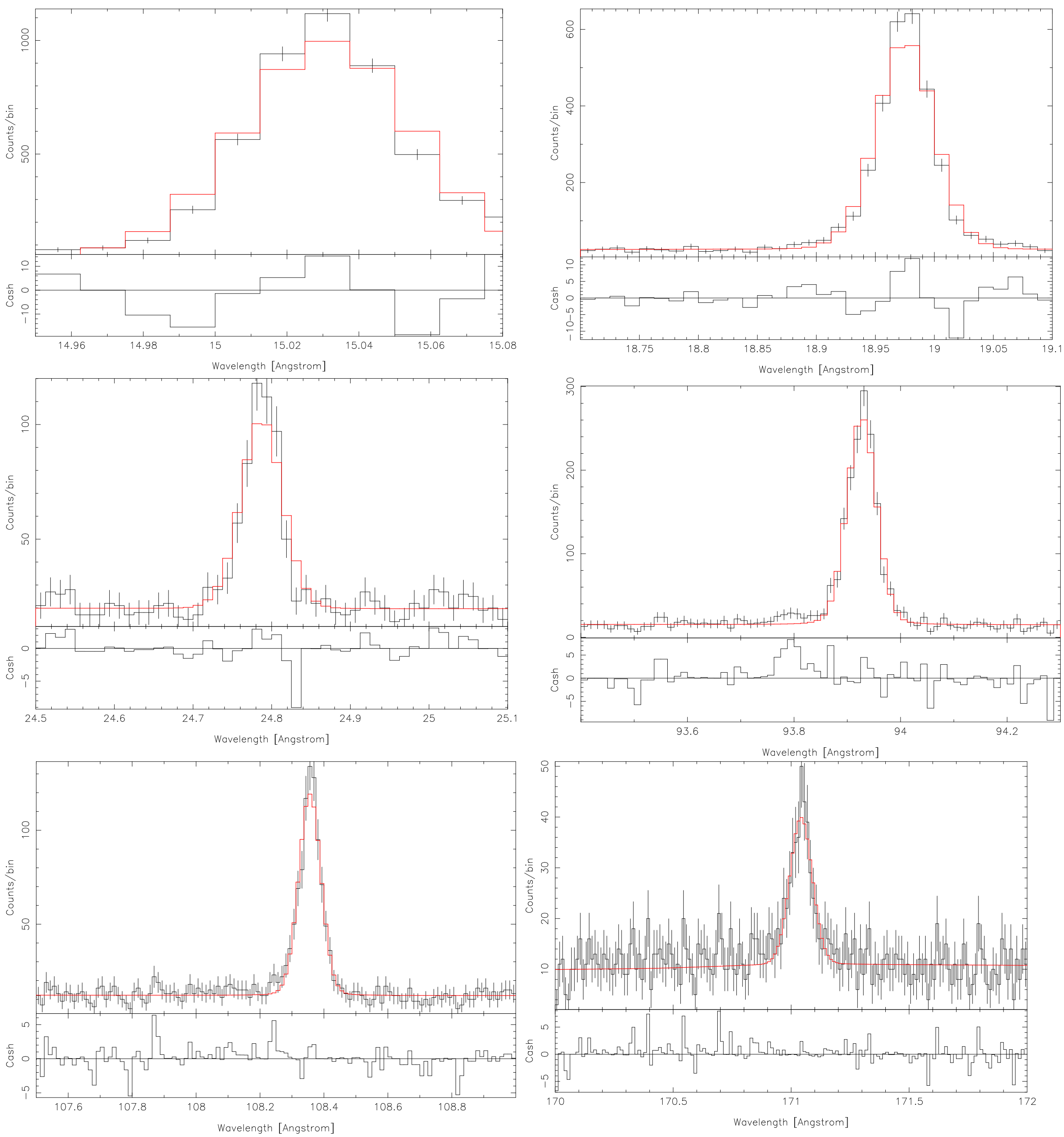

Figure 5: Selected LEG +1st-order Capella line profiles; (top left) Fe XVII line, fitted with a single Gaussian function (red; velocity width $dv \approx 42\text{km s}^{-1}$) and its goodness of fit $\chi^2 = 11.0$;(top right) O VIII ($dv \approx 9.5\text{km s}^{-1}$) with $\chi^2 = 2.86$; (middle left) N VII ($dv \approx 11\text{km s}^{-1}$) with $\chi^2 = 1.09$; (middle right) Fe XVIII ($dv \approx 33\text{km s}^{-1}$) with $\chi^2 = 1.86$; (bottom left) Fe XIX ($dv \approx 64\text{km s}^{-1}$) with $\chi^2 = 0.975$; and (bottom right) Fe IX ($dv \approx 66\text{km s}^{-1}$)with $\chi^2 = 1.12$.

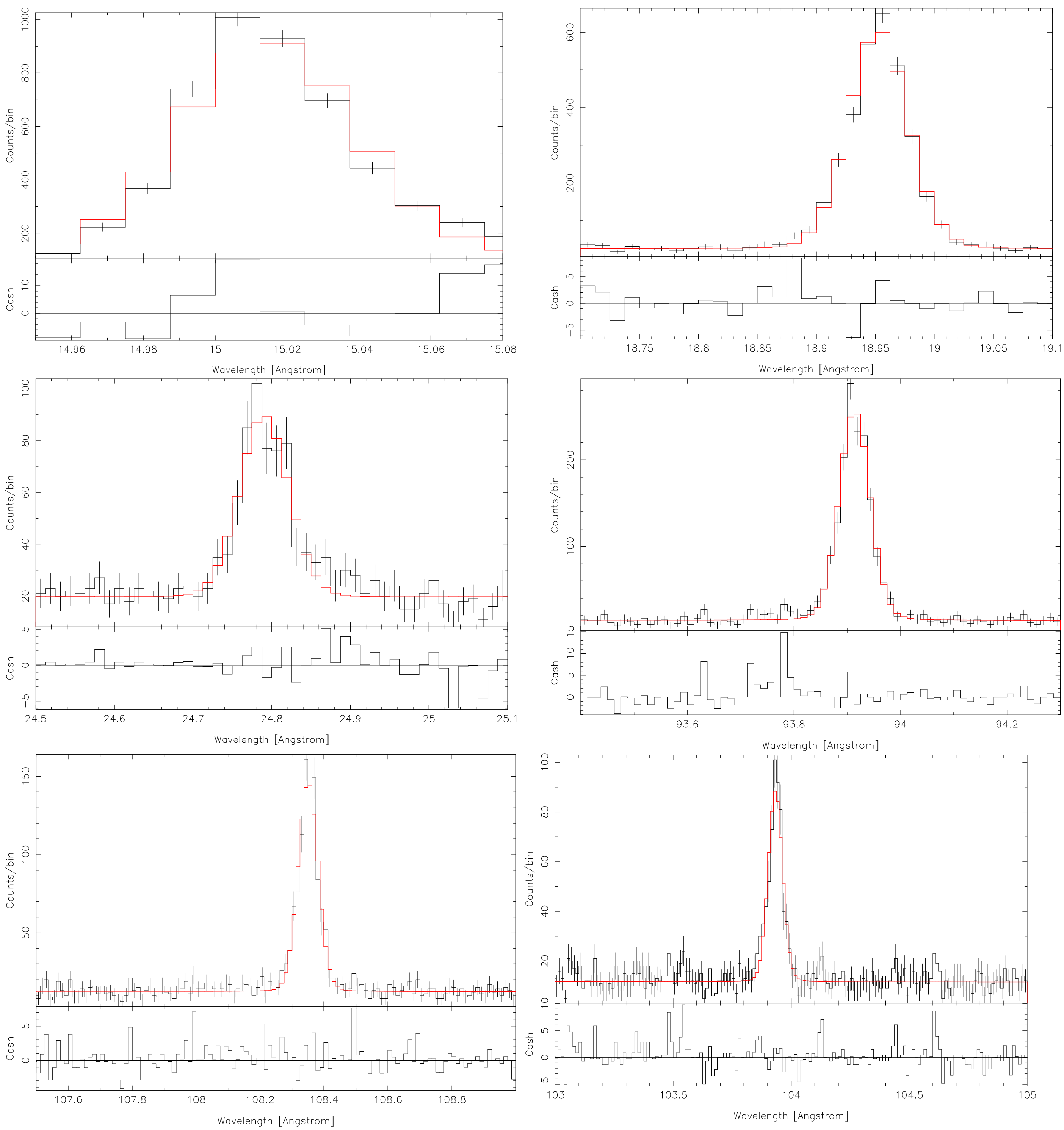

Figure 6: Selected LEG -1st-order Capella line profiles; (top left) Fe XVII line, fitted with a single Gaussian function (red; velocity width $dv \approx 3.7$km s^{-1}) and its goodness of fit $\chi^2 = 3.21$;(top right) O VIII ($dv \approx 112$km s^{-1}) with $\chi^2 = 1.72$; (middle left) N VII ($dv \approx 237$km s^{-1}) with $\chi^2 = 1.18$; (middle right) Fe XVIII ($dv \approx 45$km s^{-1}) with $\chi^2 = 1.55$; (bottom left) Fe XIX ($dv \approx 49$km s^{-1}) with $\chi^2 = 1.25$; and (bottom right) Fe XVII ($dv \approx 48$km s^{-1})with $\chi^2 = 1.44$.

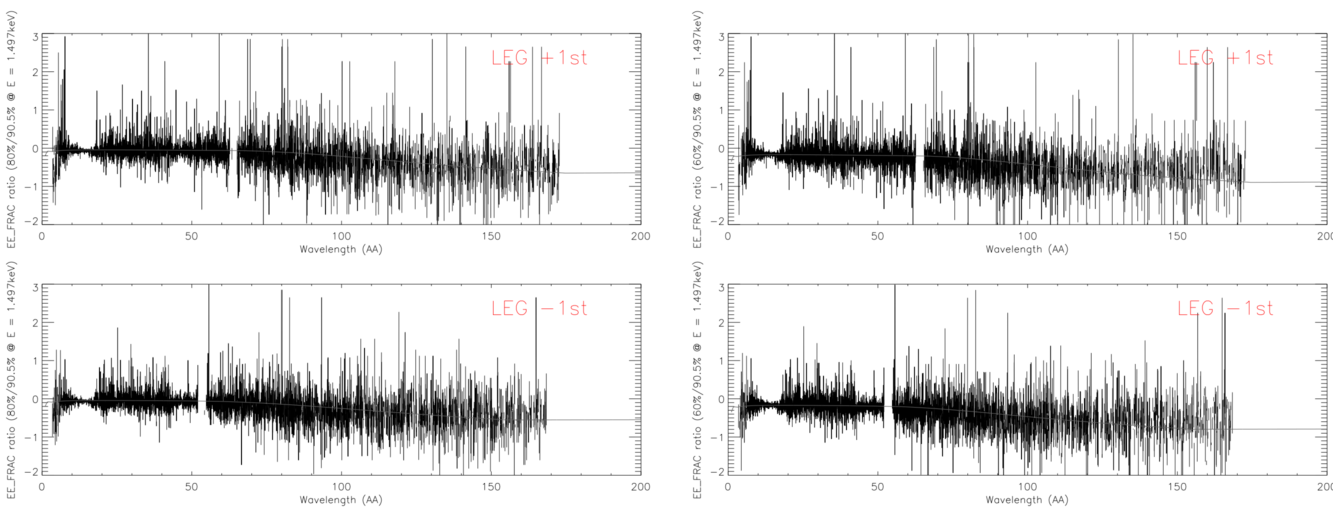

Figure 7: Ratio plots of theoretical (gray) and Capella's observed (black) EEFRAC values: (left) LEG ±1st, the ratio of Extraction B to A; (right) LEG ±1st, the ratio of Extraction C to A.